Application of Stereoscopic Particle Image Velocimetry to Experimental Analysis of Flow through Multiblade Fan*

Gyeong Rae CHO**, Masaaki KAWAHASHI***, Hiroyuki HIRAHARA*** and Michio KITADUME****

An experimental analysis of the 3D velocity field of flow is very effective for the understanding of the physical significance of complex flow and for the practical design of fluid machinery. Under the currently circumstance, stereoscopic particle image velocimetry (SPIV) is one of the promising techniques for the experimental analysis. Although the development of algorithms and the feasibility studies of SPIV have been realized, the accumulation of techniques for applications leading to the design of practical fluid machineries or devices is not yet sufficient. To establish practical techniques for the experimental analysis of 3D flow in fluid machinery by SPIV, the detailed 3D analysis of flow using a utility model of multiblade fans used in automobile air-conditioning systems has been carried out. The stereo view camera arrangement and laser-light-sheet illumination for the complex shape of the fan and for the 3D flow through it have been investigated, and the visualization of experimental results for the understanding of the flow structure has also been discussed. The results obtained using the practical techniques applied in this experiment provide knowledge useful in the understanding of flow through the fan and in improving it.

Key Words: Flow Measurement, 3D Velocity Field, Stereoscopic PIV, Multiblade Fan

1. Introduction

Although the numerical method of 3D flow analysis has been established as an essential tool for the practical design of fluid machinery, the development of experimental techniques of 3D flow field analysis is desired for the understanding of real physical phenomena and for the verification of numerical results. As the experimental methods of 3D velocity field analysis, 3D-PTV (particle tracking velocimetry) using two or three video cameras in a stereo view arrangement[1),(2)], stereoscopic PIV (SPIV)[3),(4)] and holographic PIV (HPIV)[5),(6)] have been developed. SPIV is different from the other two techniques in that it is not a volume measurement technique and it only gives three components of velocity in a plane of measurement. However, currently SPIV must be the most promising technique for 3D velocity field analysis in practical use. Therefore, many feasibility studies of SPIV including those of calibration algorithms, accuracy evaluation and practical techniques have been carried out, and also some application studies have been performed successfully[7),(8)]. However, the applications of SPIV leading to the understanding of the physical significance of complex flow structures induced in fluid machineries or to obtaining practical knowledge of the design of these structures are insufficient because of the technical difficulties caused by their complex configuration, such as moving boundaries and rotating components. The experimental analysis of 3D flow through the multiblade fan of automobile air-conditioning systems has been performed by SPIV to achieve practical SPIV techniques. In this case, there are some typical problems in 3D velocity field measurements with respect to the geometric configuration of the measurement section and the restriction of the optical arrangement. First is that the out-of-plane component of velocity in the measurement section is dominant. This corresponds to the flow at the bell-mouth opening of the scroll casing of the fan. The second is the difficulty in velocity field measurement at a hollow configuration corresponding to the inlet part of the impeller of the fan. The third one

* Received 11th June, 2004 (No. 03-4087)

** Graduate School of Science and Engineering, Saitama University, 255 Shimo-Okubo, Sakura-ku, Saitama-shi, 338-8570, Japan

*** Faculty of Engineering, Saitama University

**** SANDEN CORP., 350 Yattajima, Isesaki-shi 372-8558, Japan

is the outflow through a rotating component corresponding to the flow passing through the impeller blades. To establish practical techniques of SPIV for these cases, the measurements of the 3D inflow of the fan with a scroll casing and 3D outflow through a rotating impeller without a scroll casing were carried out.

The multiblade fan is one of the well-investigated fluid machinery, and its fundamental design concept is established well. However, in the recent situation of high-level requirement on the living environment such as high flowrate and efficiency, a new design concept of the multiblade fan directed to the reduction in aero-acoustic noise has become important. There are many sources of the noise induced in the fan. Wu and Bai[9] recently reported that the noise generated by centrifugal fans falls into two categories corresponding to the blade passing frequency noise with discrete or narrow-band frequency components and the turbulent noise in the cut-off region of the casing. They also attempted to reduce blade passing frequency noise by the active-noise control technique. However, to reduce the other noise factors, the detailed analysis of the flow through the fan is necessary. The effectiveness of the conventional PIV for velocity field measurement of the blade passage flow of the impeller has been shown by Kawahashi et al.[10] The results showed the flow separation in the suction side of blade passage and its change in the spanwise direction with scroll angle. The results provided knowledge useful in examining the shape of the blade. The 3D velocity field analysis of the flow through the fan by SPIV brings more information on the global design of multiblade fans. However, in the SPIV of the flow through the fan, there are some difficulties in the optical arrangement because of the complexity of the shape.

In this study, the practical techniques of SPIV measurements of the inflow and outflow through the impeller of the fan, such as the arrangement of cameras, the calibration technique for reconstructing the three components of velocity, the phase-locking measurement of flow around a rotating impeller, have been established. In particular, in the case of velocity field measurements in the inlet part of the impeller, a modified optical arrangement of SPIV was introduced. SPIV by a phase locking technique was carried out to measure the outflow through the impeller, and the 3D flow structure caused by separation in blade passage and the wake of blades has been clarified. The establishment of experimental techniques for 3D flow analysis can lead to a better understanding of the flow through the fan for improvement in the design of the impeller, such as blade shape and blade setting angle.

2. SPIV Method

A schematic view of the SPIV system with a standard optical arrangement is shown in Fig. 1. The measurement plane is illuminated by a laser light sheet issuing from

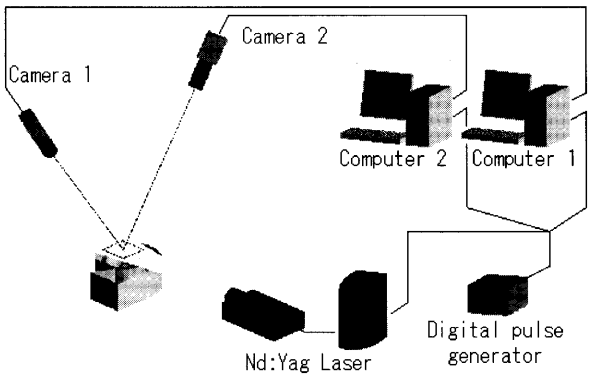

Fig. 1 Schematic view of SPIV system

double-pulsed Nd:YAG lasers, and the thickness of the light sheet is 2 mm. Two CCD cameras with $1\,008 \times 1\,016$ pixels are arranged for stereo viewing on the same side against the light sheet, and are synchronized to the pulsed lasers by a digital pulse generator.

In fluid machinery, the 3D flow analysis of hollow parts is a major problem. In the application of SPIV to this case, there are some difficulties in the optical pass of laser illumination and stereoscopic viewing angle of the cameras, thus the optical arrangement shown in Fig. 1 cannot be applied. In this investigation, two types of optical arrangement in Fig. 2 (a) and (b) have been applied, and accordingly two different calibration methods using the same type of calibration plate shown in Fig. 2 (c) were carried out. The calibration plate has 30×30 white grid lines with a 0.2 mm thickness and a 3 mm line-to-line spacing on a black surface. Figure 2 (a) shows the standard arrangement of SPIV in which the calibration plate was set parallel to the plane of measurement and was moved perpendicular to the plane. Figure 2 (b) shows the modified arrangement in which each camera was set on both sides of the measurement plane. In this case, the calibration plate cannot be located in the same direction as in the former case. Thus, it was set perpendicular to the plane and moved in the direction along the plane. However, in this case, the problem of accuracy in the calibration process still remains. Moreover, it is possible to avoid the problem using a transparent and thin calibration plate or a thin calibration plate having exactly the same patterns on both sides. However, the second arrangement is applied to the measurement of the hollow part. This arrangement has a defect in focusing within a whole image plane because of the small viewing angle of the camera for the laser light sheet. It will increase the rate of erroneous vectors, but this can be improved using a Sheimpflüg configuration, which enables us to focus on the whole region of observation by changing the optical angle between the lens and image plane of the camera. The calibration processes for both optical arrangements have been described by Prasad[11].

The coordinate transformation between the image

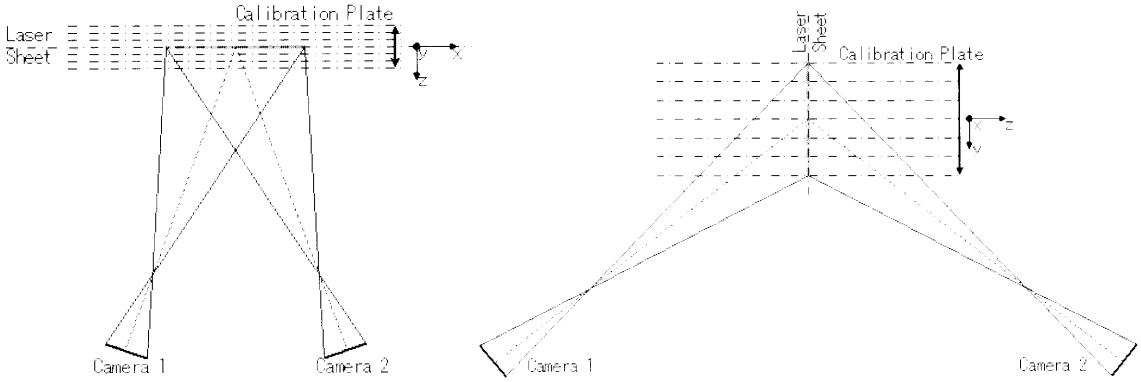

(a) Standard setup (b) Modified setup

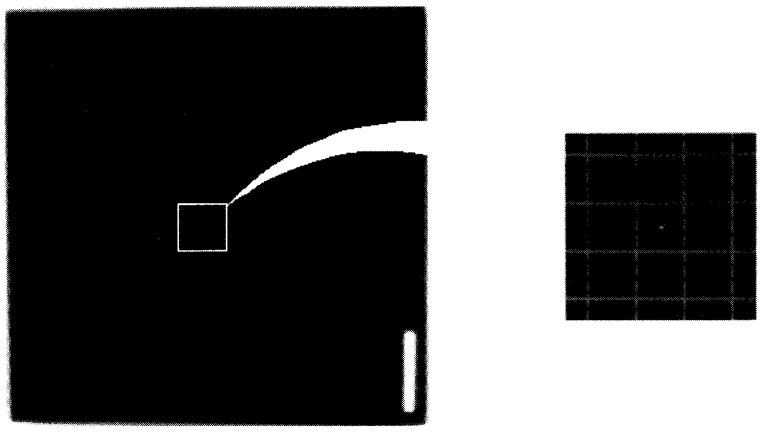

(c) Calibration plate with grid lines

Fig. 2 Optical setup of stereoscope system

plane and the object field for reconstruction of the 3D velocity vector field from stereoscopic images has been performed using the following equations based on the geometric relationship between the image plane (X,Y) and the object field (x,y,z) proposed by Doh et al.[12].

$$F_X = c_X \frac{x_m - m_x}{\sqrt{d_0^2 - m_x^2 - m_y^2 - z_m}} - (X - \Delta X) = 0 \qquad (1)$$

$$F_Y = c_Y \frac{y_m - m_y}{\sqrt{d_0^2 - m_x^2 - m_y^2 - z_m}} - (Y - \Delta Y) = 0 \qquad (2)$$

Where, F is the mapping function (observation equation) relating the object field position (x,y,z) to the image plane position (X,Y) of the camera. c is the magnification factor and d_0 is the distance between the camera and the original point of the object field. The symbol m denotes the axial deviation between Z and z', where Z is the out-of-image axis and z' is the three-dimensionally rotated z axis to adjust axes deviation between the image plane and the object field. ΔX and ΔY are the lens refractions on the image. The subscript m denotes the three-dimensionally rotated point of (x,y,z). All these parameters were calculated by an improved Gauss-Newton method, and 3D physical positions were obtained at the intersection point of two lines tracing the particle point on the image and the camera center, that is, the focal point of the camera lens, for both images and cameras. This algorithm was applied to both optical arrangements. Using the camera information, 3D vectors were directly reconstructed from two vector maps obtained by the cross-correlation of two sequential images captured using both cameras.

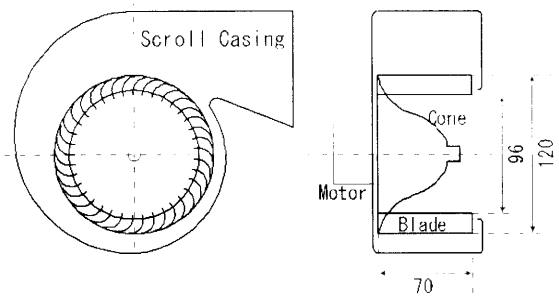

Fig. 3 Configuration of multiblade fan

3. Measurement of Inflow of Fan

3.1 Experiment apparatus and method

The measurements have been performed on a multiblade fan of compact size shown in Fig. 3. The impeller of the fan has a bell-shaped motor cover, called cone, at the center. The impeller has 37 blades, and the outer diameter, inner diameter and blade span are 120 mm, 96 mm,

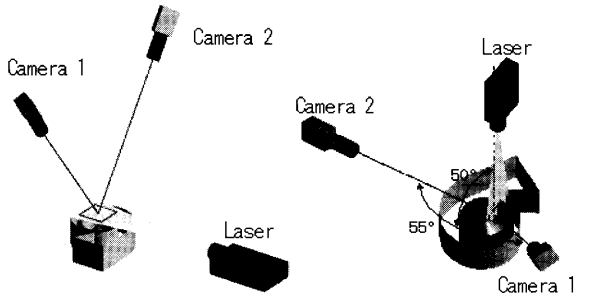

(a) Measurement in horizontal sections upstream of the bell-mouth

(b) Measurement in radial sections in the inlet part of the impeller

Fig. 4 Experimental setup of SPIV measurement

and 70 mm, respectively. The revolution speed of the impeller was kept at 2 000 rpm (the outer and inner circumferential speeds were about 12.57 m/s and 10.05 m/s) in the measurements. The fan performance was measured with JIS-B8330. The volume flow rate was measured with an orifice-type flowmeter. The experimental conditions were determined at a flow rate with the maximum pressure coefficient in the fan performance diagram plotted in this measurement.

First, SPIV was applied to the measurement of flow at the fan inlet. The measurement section was a $110 \times 110\,\mathrm{mm}^2$ area located upstream of the bell-mouth opening as shown in Fig. 4 (a) or a $50 \times 70\,\mathrm{mm}^2$ area at eight radial sections in the inlet part of the impeller as shown in Fig. 4 (b). In the former case, the standard optical arrangement of SPIV in Fig. 2 (a) was applied to obtain 3D velocity components. In this case, the angle between the cameras and the laser sheet was about 70 degrees and the measurement plane illuminated by the laser light sheet of 2 mm thickness was 4 mm apart from the upper wall of the casing. In the latter case, the modified optical arrangement in Fig. 2 (b) was applied, because the impeller of the fan prevented the standard setting of the cameras for the stereo viewing of the measurement section. The optical angle between the two cameras was about 55° and inclined by 50° toward the center point of the impeller as shown in Fig. 4 (b). In this arrangement, by comparing the correct positional data with the recovered positional data, the standard deviation of the 3D geometrical measurement was estimated as 0.03 and 0.05 in the two in-plane directions and 0.03 mm in the one out-of-plane direction. The deviation came from a defocus effect, and is on the order of several percent with respect to the size of the measurement plane.

3.2 Results and discussion

In general, instantaneous velocity vector maps obtained by the SPIV method include some spurious or erroneous vectors. To enhance its performance, some post-processing steps for the detection and correction of erroneous vectors are required, and various methods of eliminating erroneous vectors have been proposed. In this

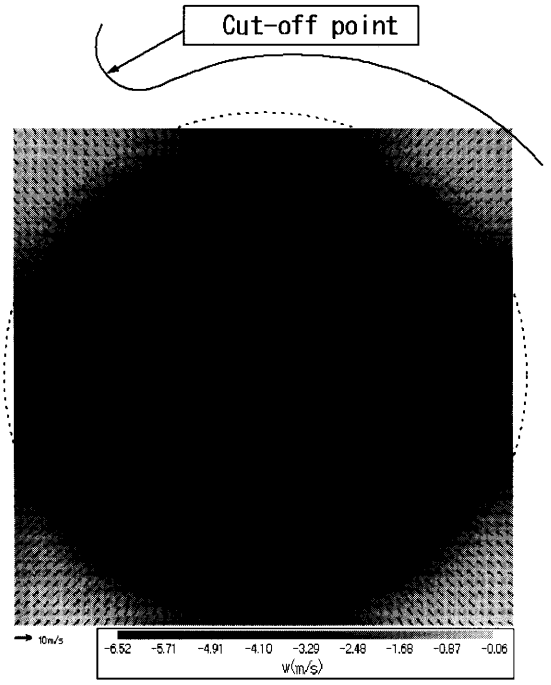

Fig. 5 Ensemble-averaged velocity map on upstream side of bell-mouth opening of casing

paper, the following equation introduced by Nogueira[13] was applied to the detection of erroneous vectors.

$$C = \frac{\sum_i |v_i - v_0|}{\sum_i |v_i|} \tag{3}$$

Where v_0 is the velocity at the examination point and v_i refers to the velocity at adjoining grid node points. C denotes the velocity variation from the velocity expected in the local velocity field and depends largely on the flow pattern of fluid. In this paper, this equation was extended to a 3D calculation for SPIV results. To detect erroneous vectors, 24 neighbor vectors were used and the threshold value was set at 0.2 (20%). The detected erroneous vectors were replaced with vectors evaluated by linear interpolation.

The ensemble-averaged 3D velocity distribution obtained using more than 300 instantaneous velocity distributions measured upstream of the bell-mouth opening of the fan is shown in Fig. 5. The velocity vectors shown in the figure are composed of in-plane velocity components and the gray level contours indicate the magnitude of out-of-plane velocity components. To indicate relative positions, the location of the cut-off, bell-mouth opening and the impeller shape are illustrated in the figure by solid and dotted lines, respectively. The figure shows that the out-of-plane component of velocity corresponding to the inflow velocity through the bell-mouth opening becomes maximum in the vicinity of the edge of the opening, and decreases toward the center. In the circumferential direction, the inflow velocity at the cut-off of the casing becomes

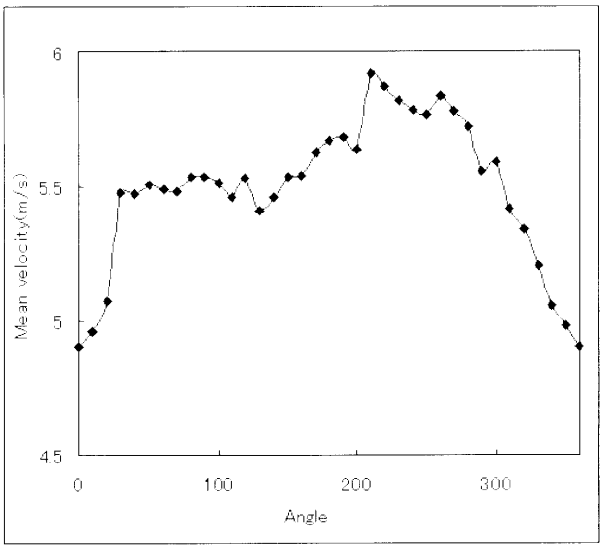

(a) Mean velocity distribution of inflow in circumferential direction

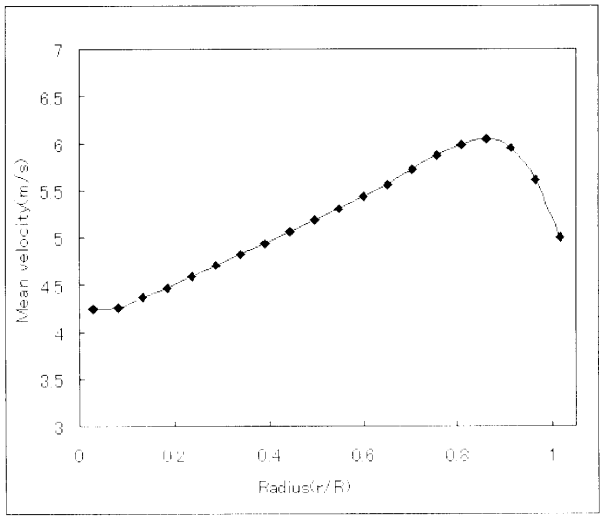

(b) Mean velocity distribution of inflow in radial direction

Fig. 6 Mean velocity distribution of inflow passing through bell-mouth opening

minimum. The distribution of the mean velocity averaged in small sections of the opening divided into fan-shaped areas with a central angle of 10° is shown in Fig. 6 (a). In this figure, the horizontal axis indicates the clockwise angle measured from the cut-off of the casing. The distribution indicates the change in inflow rate in the circumferential direction. The mean velocity becomes a minimum at the cut-off of the casing and increases rapidly at approximately 30°. The maximum mean velocity appears at approximately 210° and then decreases gradually toward the cut-off. Figure 6 (b) shows the distribution of the inflow velocity averaged along circle lines at constant radii. In the figure, r is the radius from the center of the impeller and $R(=50\,\text{mm})$ is the radius at the inner edge of the casing.

From this figure, the distribution of the inflow velocity in the radial direction at the bell-mouth opening can be seen clearly. The inflow through the bell-mouth opening is directed toward the inlet of the impeller. The spanwise velocity distribution at the inlet and the attack angle of the inflow with respect to the blade are important factors when considering the blade-passage flow. The 3D velocity field in the inlet part of the impeller has been analyzed by the SPIV method based on the optical arrangement shown in Fig. 2 (b). The measurements of 3D velocity components in the radial sections at different clockwise angles from the cut-off of the casing have been carried out. Figures 7 (a) – (d) show the ensemble-averaged velocity fields over 500 instantaneous velocity field data at 0, 45, 225 and 315° from the cut-off. These figures show in-plane velocity vector maps, and the gray level contours indicate the out-of-plane velocity component. The out-of-plane velocity component of the inflow is very small in most part of the measurement section. At 90 – 250°, a positive out-of-plane component less than 1 m/s is observed at the upper part of the cone, and at 270 – 45°, a negative out-of-plane component is observed. However, this is not significant for the inflow structure. However, at 0 and 45°, strong out-of-plane velocity component is observed in the lower part of the impeller as shown in Fig. 7 (a) and (b). This suggests that the inflow in the vicinity of the cut-off is affected by the complex flow configuration at the cut-off

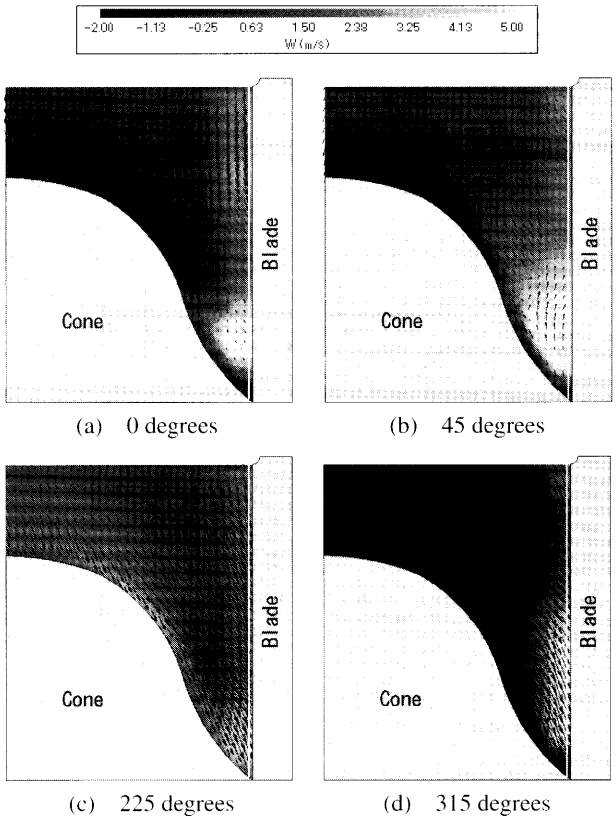

Fig. 7 Ensemble-averaged velocity maps at four different scroll angles measured from cut-off

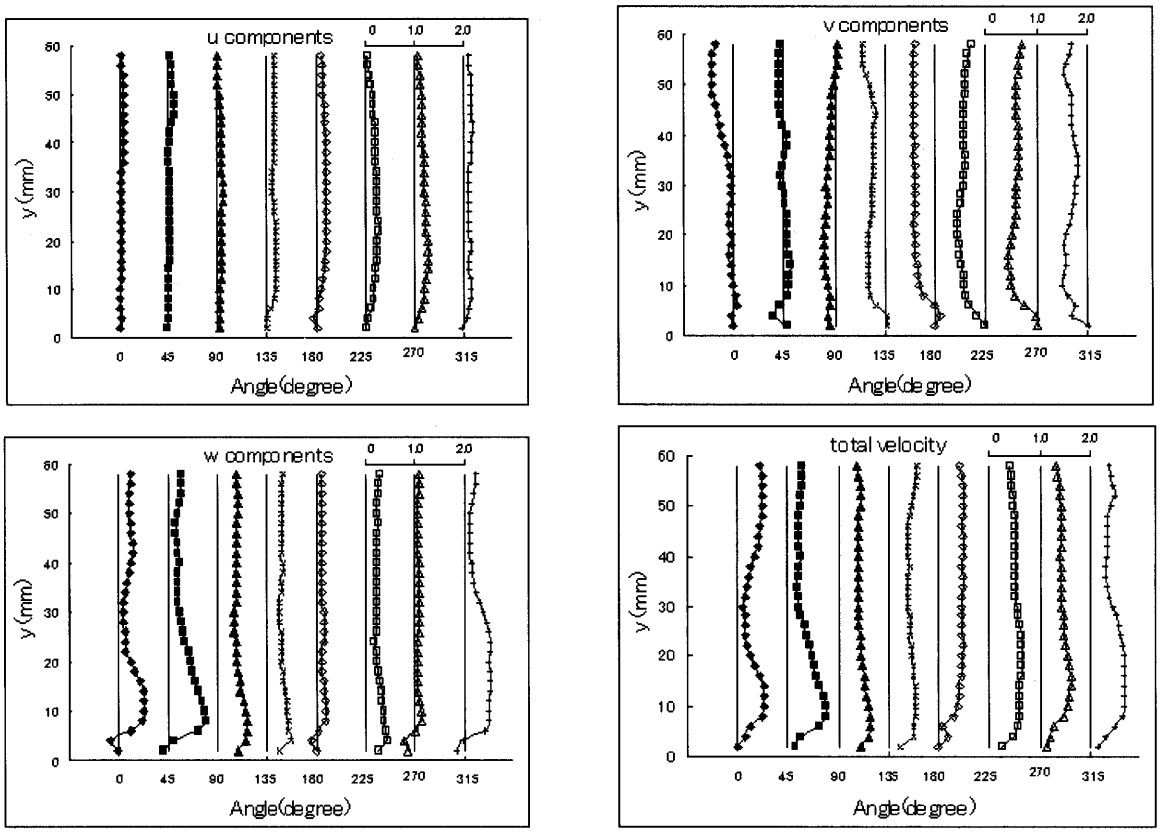

Fig. 8 Profiles of velocity components 1 mm in front of leading edge of impeller blade

of the casing. This 3D structure in the lower part of the impeller disappears with increasing clockwise angle. Figure 8 shows the profiles of each velocity component along lines at 1 mm from the leading edge of the impeller blades for different scroll angles. These lines are indicated by white lines in Fig. 7. The velocity components u, v and w are radial, axial and circumferential, respectively. These velocity components have been normalized by the circumferential velocity of 10.05 m/s at the inner edge of the impeller. The results show that the flow just in front of the impeller inlet has a large velocity component in the circumferential direction and the distributions of u, v and w components change markedly with scroll angle. This means that the characteristics of the blade passage flow are different in the circumferential direction and the flow rate through the impeller also differs in this direction. The lower-part distributions of the v component at 0 and 45° correspond to the flow structure observed in Fig. 7 (a) and (b). From these results, it can be summarized that the flow in the inlet part of the impeller has a complex 3D structure and the blade-passage flow through the impeller changes with position in the circumferential direction.

For better understanding of the 3D inflow structure of the fan, a visual illustration of the obtained data must be effective. For this purpose, 3D velocity data of 24 radial sections from 15 to 345° has been derived using the Spline interpolation of SPIV measurement results in 8 radial sections. The streamlines generated by the 3D velocity field data are illustrated in Fig. 9. The coordinates of the center axis and radial direction are indicated by y and r. The position of the cut-off is indicated by a white line on the cone surface of the impeller, and the angle of view is measured from the cut-off position. This figure shows a strong 3D flow configuration around the cut-off, and smooth streamlines without significant precirculation in the inlet part of the impeller are observed at 180 – 270°. These results suggest that the cut-off of the casing causes the generation of 3D structures in the inflow in the scroll angle range of 0 – 90°, and affects the blade-passage flow through the impeller and the flow field in the casing. To improve this situation, the geometry of the cut-off of the casing must be improved.

4. Measurement of Outflow from Impeller

4.1 Measurement setup

The next target of the SPIV measurement is the outflow from the rotating multiblade impeller. The flow field shows an unsteady and 3D turbulent structure caused by the blade-passage flow with separation and the shear layer in the wake of the blade. To analyze the flow field, an SPIV measurement combined with a phase locking technique is suitable for determining averaged velocity fields at different blade positions in the circumferential direction, and the visual reconstruction of 3D velocity fields is

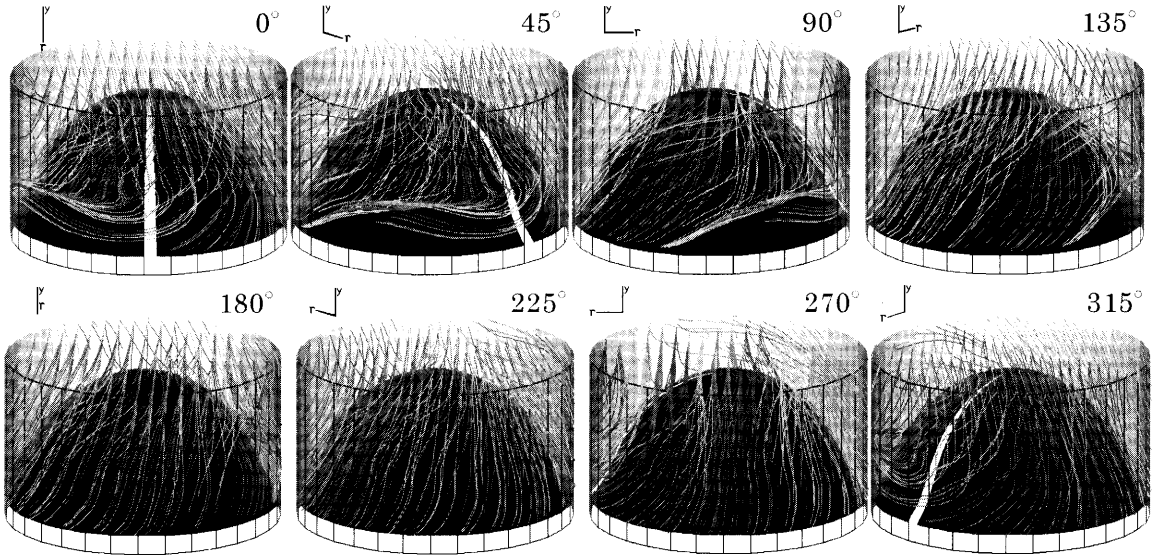

Fig. 9 Streamlines of 3D flow field in inlet part of impeller

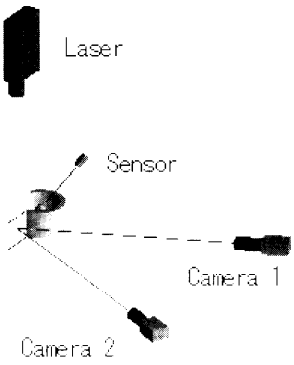

Fig. 10 Experimental setup for measurement of outflow passing through impeller

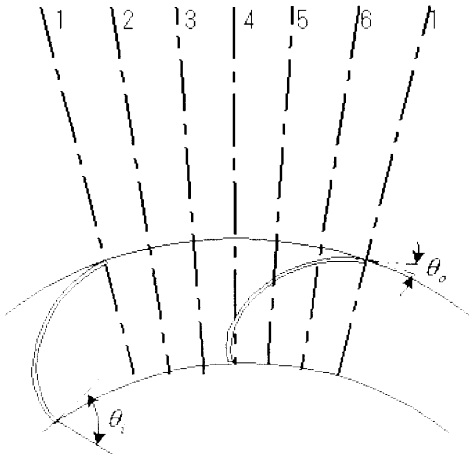

Fig. 11 Radial sections of outflow measurement for six phases of blade position

useful in the understanding of flow structures. To establish and confirm the effectiveness of these methods of experimental analysis, measurements have been carried out for the case without a casing. In a global analysis of the flow through a fan, the effect of a casing must be considered; however some experimental difficulty in the SPIV measurement using a casing still remains because of the refraction induced by the curved wall of the casing, pollution of the inside wall by tracer particles, calibration and so on. In this paper, the measurement without a casing has been conducted to confirm the fundamental features of the outflow from a rotating impeller.

The standard arrangement of SPIV shown in Fig. 10 can be used for the above measurement. A photocoupler was used for generating phase locking signals at an accuracy of 0.1°. The measurement has been carried out at six phases of the blade position within the range of one blade interval of the impeller as shown in Fig. 11, and 3D velocity components in the radial sections in the periphery of the impeller were obtained. In Fig. 11, θ_i and θ_o are the inlet and outlet setting angles (68° and 30°) of the blade, respectively. The ensemble-averaged 3D velocity map has been reconstructed from the data obtained at each phase.

4.2 Results and discussion

Figure 12 shows an instantaneous velocity vector map in the periphery of the impeller at phase 1 of Fig. 11. In this figure, strong out-of-plane velocity components in lower part of the blade, a complex 3D structure of the outflow and a reversed flow in the upper part of the blade are observed clearly. Figure 13 shows a map of equivelocity surfaces reconstructed by the interpolation of the ensemble-averaged velocity fields measured at six phases of the blade position. The main part of the outflow is concentrated in the lower part of the impeller and the maximum velocity is 13.16 m/s, which is about 1.05 times of the circumferential velocity of the outer edge of the impeller.

Ensemble-averaged absolute velocity profiles at each phase within one blade interval at 8 different heights in

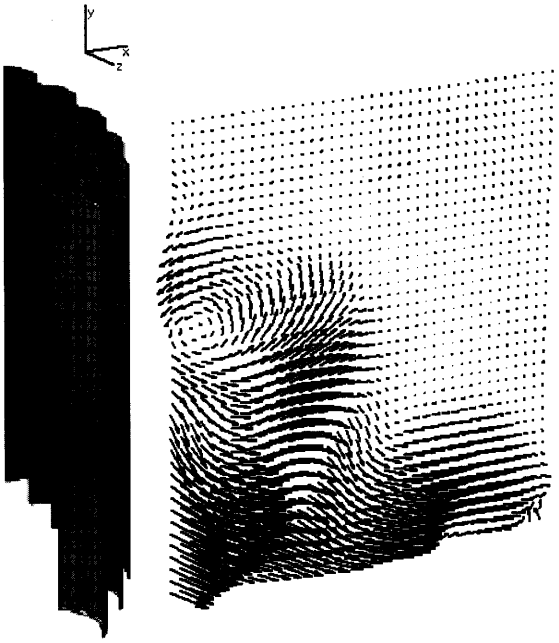

Fig. 12 Instantaneous velocity vector map of outflow passing through impeller at phase 1

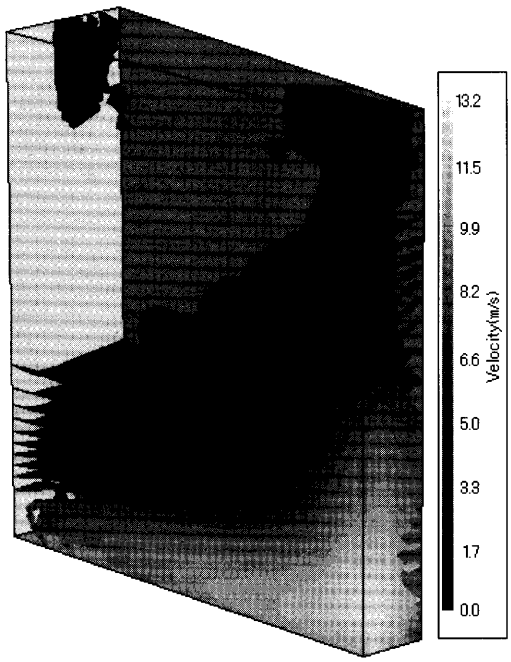

Fig. 13 Three-dimensional equivelocity surfaces of outflow reconstructed by SPIV measurements by phase locking technique

spanwise direction of the blade are shown in Fig. 14. The velocity was measured 1 mm from the rear of the trailing edge at each phase of the blade position. H is the blade span and y is the position in the spanwise direction. V_0 is the circumferential velocity of the outer edge of the impeller, and was about 12.6 m/s. The figure shows the variation of velocity profiles in the spanwise direction. At the lowest end ($y/H = 0$), the maximum velocity appears

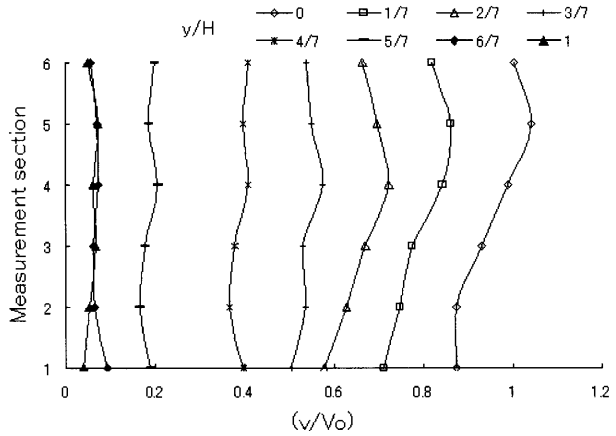

Fig. 14 Ensemble-averaged absolute velocity profiles of blade passage flow at different spanwise positions

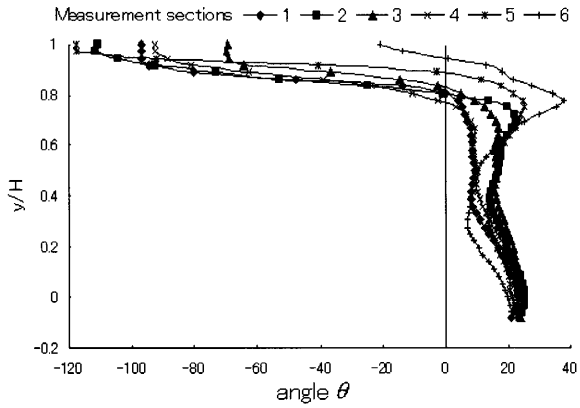

Fig. 15 Spanwise distribution of outflow angle at 1 mm rear of impeller for different phases of blade position

on the pressure side and its value exceeds V_0. As y/H increases, the point of maximum velocity moves toward the center of the blade passage and its value decreases. Figure 15 shows the spanwise distributions of the outflow angles at 1 mm rear of the impeller for different phases of blade position. The outflow angle related to the fan performance is evaluated based on the ensemble-averaged velocity vector map

$$\theta = \tan^{-1}(u/w), \tag{4}$$

where u and w are the velocity components in the radial and rotational directions of the impeller. The angle in the lower part of the blade is equivalent to the outlet setting angle of the blade. The angle in the upper half part varies markedly in the circumferential direction. The results suggest the complex configuration of the flow through the blade passage such as separation on the suction side, recirculating flow by the shroud separation and the wake of the blade. There is a limit in considering the effect of a scroll casing on the outflow from a rotating impeller. However, the results give some information and knowledge useful in estimating fundamental characteristics of the impeller and in examining the effects of blade shape.

5. Conclusion

SPIV measurement of inflow and outflow through the impeller of a multiblade fan have been successfully carried out.

The results of the inflow measurement in the bell-mouth opening section of the casing show non-axisymmetric distribution of inflow rate. The velocity field measurements in the inlet part of the impeller clarified 3D flow structures by means of the streamlines reconstructed by postprocessing of the 3D velocity components data obtained by SPIV measurement. Then, SPIV measurement experiments by a phase-locking technique have been performed on the unsteady and turbulent outflow through a rotating impeller. From the results obtained, ensemble-averaged 3D flow structures are reconstructed by illustrating equivelocity surfaces.

The results obtained in this report may contribute to the extension of the applicability of SPIV to the experimental analysis of 3D velocity fields in various practical situations.

Acknowledgements

The authors would like to express many thanks to Mr. T. Uchida for his assistance in the experiments.

References

(1) Chang, T.P.K., Watson, A.T. and Tatterson, G.B., Image Processing of Tracer Particle Motions as Applied to Mixing and Turbulent Flow I, Chemical Engineering Science, Vol.40, No.2 (1985), pp.269–275.

(2) Nishino, K., Kasagi, N. and Hirata, M., Three-Dimensinal Particle Tracking Velocimetry Based on Automated Digital Image Processing, Transactioons of ASME, Journal of Fluids Engineering, Vol.111 (1989), pp.384–391.

(3) Arroy, M.P. and Greated, C.A., Stereoscopic Particle Image Velocimetry, Measurement Science and Technology, Vol.2 (1991), pp.1181–1186.

(4) Prasad, A.K. and Adrian, R.J., Stereoscopic Particle Image Velocimetry Applied to Liquid Flows, Experiments in Fluids, Vol.15 (1993), pp.49–60.

(5) Meng, H. and Hussain, F., Holographic Particle Velocimetry (A 3D Measurement Technique for Vortex Interaction, Coherent Structure and Turbulence), Fluid Dynamic Research, Vol.8, Nos.1-4 (1991), pp.33–52.

(6) Barnhart, D.H., Adrian, R.J. and Papen, G.C., Phase-Conjugate Holographic System for High-Resolution Particle-Image Velocimetry, Applied Optics, Vol.33, No.30 (1994), pp.7159–7170.

(7) Hill, D.F., Sharp, K.V. and Adrian, R.J., Stereoscopic Particle Image Velocimetry Measurements of the Flow around a Rushton Turbine, Exp. in Fluids, Vol.29 (2000), pp.478–485.

(8) Hu, H., Saga, T., Kobayashi, T., Taniguchi, N. and Yasuki, M., Dual-Plane Stereoscopic Particle Image Velocimetry: System Setup and Its Application on a Lobed Jet Mixing Flow, Exp. in Fluids, Vol.31 (2001), pp.277–293.

(9) Wu, J.D. and Bai, M.R., Application of Feedforward Adaptive Active-Noise Control for Reducing Blade Passing Noise in Centrifugal Fans, Journal of Sound and Vibration, Vol.239, No.5 (2001), pp.1051–1062.

(10) Kawahashi, M., Satou, S., Fujita, Y. and Yamamoto, K., Experimental Flow Analysis of a Multi-Blade Fan Being Used for Automobile Air-Conditioner, Proc. Seoul 2000 FISITA, World Automobile Congress, F2000H199, (2000), pp.1–7.

(11) Prasad, A.K., Stereoscopic Particle Image Velocimetry, Exp. Fluids, Vol.29 (2000), pp.103–115.

(12) Doh, D.H., Kim, D.H., Cho, K.R., Cho, Y.B., Lee, W.J., Saga, T. and Kobayashi, T., Development of Genetic Algorithm Based 3D-PTV Technique, Journal of Visualization, Vol.5, No.3 (2002), pp.243–254.

(13) Nogueira, J., Lecuona, A. and Rodriguez, P.A., Data Validation, False Vectors Correction and Derived Magnitudes Calculation on PIV Data, Measurements of Science and Technology, Vol.8 (1997), pp.1493–1501.